Coherent Radiation Spectrum Measurements at KEK LUCX Facility

M. Shevelev[a,*], A. Aryshev[a,*], S. Araki[a], M. Fukuda[a], P. Karataev[b], K. Lekomtsev[a], N. Terunuma[a], J. Urakawa[a]

[a] *KEK: High Energy Accelerator Research Organization,1-1 Oho, Tsukuba, Ibaraki 305-0801, Japan*

[b] *John Adams Institute at Royal Holloway, University of London, Egham, Surrey, TW20 0EX, United Kingdom*

Abstract

In this paper we demonstrate the detailed design concept, alignment and initial test of a Michelson interferometer for THz spectral range. The first coherent transition radiation spectrum measurement results and ultra-fast broadband room temperature Schottky barrier diode detectors performance are presented. The main criteria of interferometer beam splitter optimization, motion system high precision calibration and its linearity check as well as alignment technique are discussed.

Keywords: Coherent transition radiation, THz radiation, Michelson interferometer

1. Introduction

In the last decade electromagnetic radiation in the terahertz frequency domain has started playing a key role in different applications ranging from material and biomedical science to quality control and national security [1, 2, 3, 4, 5]. Recent advances in these studies have encouraged an interest in investigation and development of THz radiation generation methods. One of the research directions in THz science and technology [6, 7, 8] is to generate short and high-brightness THz-frequency coherent radiation pulses

*Corresponding authors

Email addresses: mishe@post.kek.jp (M. Shevelev), alar@post.kek.jp (A. Aryshev)

Preprint submitted to Nuclear Inst. and Methods in Physics Research, A March 27, 2014

using ultra-short electron bunches of a compact accelerator. The intensity of this radiation is proportional to the square of the beam current. For a stable THz emission one should consider generation of electron bunches with the duration smaller than 100 fs (about 30 μm) and the intensity stability of $< 1\%$ rms. One possibility to obtain such short electron bunches is to illuminate a photo-cathode of an RF-Gun with a femtosecond laser pulse. In this case a well-established on-line diagnostics and control of both the laser and the electron beams are needed. Recent progress in laser technology and ultra-short laser pulse diagnostics [9, 10] gives promising results whereas reliable methods for determination of femtosecond electron bunches still have to be developed. A streak camera [11] can provide about 300 fs resolution which is not applicable in this case. On the other hand deflecting cavity [12, 13, 14] can give required resolution but it makes an inadmissible problem for a "table-top" accelerator based THz source design since the change related to accelerator high power RF distribution system and a significant beamline space allocation are required for the installation. Alternatively Electro-Optic methods for longitudinal bunch diagnostics [15] requires complex apparatus involvement and careful calibration.

Another promising technique for longitudinal bunch shape reconstruction is based on the coherent radiation spectral density distribution measurement [16, 17, 18, 19, 20]. Unfortunately this method is likely to have some restrictions and limitations which should be considered in detail to push forward a progress in this direction.

As a potential candidate for spectrometry of the intense broadband radiation in THz and sub-THz frequency range and for longitudinal bunch shape reconstruction the Michelson interferometer (MI) was constructed as a part of a larger THz program launched at KEK LUCX (Laser Undulator Compton X-ray) facility [21, 22, 23]. The program aims to investigate various mechanisms for generating EM radiation including stimulated coherent diffraction radiation, undulator radiation, Smith-Purcell radiation and other types of polarization radiation.

In this paper we demonstrate a detailed design concept, alignment and initial MI test for the THz spectral range. The first coherent transition radiation spectrum measurement results and the ultra-fast broadband room temperature Schottky barrier diode detector performance are presented.

2. Michelson interferometer for THz spectral range

The MI is the most common configuration for optical interferometry which can be extended to a long wavelength range including THz and IR [16, 24]. Its design is much simpler than so-called Martin-Puplett interferometer [25, 26, 27, 28] since only one detector is required and no wire grid polarizers are used. Also it does not require any special alignment techniques what significantly increases measurements quality. Moreover the same interferometer can be aligned with optical wavelengths and used for THz spectroscopy with only beam splitter (BS) replacement. A general MI layout for THz spectral measurements is given in Fig.1.

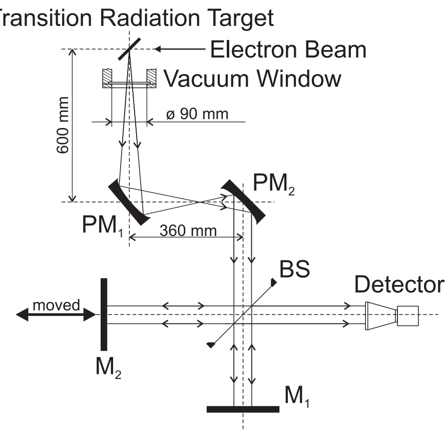

Figure 1: General layout of Michelson interferometer and THz radiation transport line.

An interference pattern is produced by splitting a beam of light into two paths, reflecting beams back and recombining them through the splitter again. The setup consists of a THz radiation transport line (RTL), beam splitter (BS), two interferometer arms formed by two flat aluminum mirrors (M1 and motorized M2 mirror), alignment system, THz polarizer and the detector. The incident THz wave propagates through the vacuum window (VW) and RTL, which consists of two off-axis parabolic mirrors (PM1 and PM2). After that it is divided by the BS so that one half of the incoming intensity is transmitted through BS towards M1 and the other half is reflected from BS towards M2. The BS was installed at the center of the interferometer at 45 degree with respect to the radiation beam axis. The radiation beams are then reflected by the flat mirrors (M1 and M2) and reach the beam splitter again. To acquire autocorrelation dependence (interferogram), the mirror (M2) was moved along the optical axis of the interferometer perpendicular arm back and forth. The flat optical-grade 100 mm diameter, 15 mm thickness and $\lambda/4$ surface flatness aluminum mirrors (Sigma-koki TFAN-100C15-4) were used along with optical mirror mounts (Sigma-koki MHA-100S [29]). The distance between the BS and the fixed mirror M1 was 200 mm. The main MI components including BS, motion system, alignment system and the THz detection system will be presented in details below.

2.1. Beam splitter

Beam splitter determines the intensity and polarization features of the radiation for both arms of the interferometer which influences the quality of the interferogram. In modern MIs polyethylene terephthalate (PET or Mylar) beam splitters are widely used. The Maylar is commercially available. However, the efficiency of PET beam splitters strongly depends on thickness and radiation wavelength therefore for a wide-spectrum study usually a set of Maylar splitters is needed [30]. Recently it has been shown that the Silicon splitter efficiency is much higher than for the PET splitters in terahertz region [31]. Silicon is a well-known material. It has a negligible absorption coefficient and high refractive index in broadband THz range [32, 33]. It is important to point out that the theoretical efficiency for a beam splitter is given by $\varepsilon = 4R_0T_0$, where R_0 and T_0 are the reflectance and transmittance of the beam splitter which are the functions of incident angle, refractive index and a thickness of a splitter [34]. The maximum efficiency can be obtained when $R_0 = T_0 = 0.5$, in this case $\varepsilon = 1$.

The main criteria of beam splitter optimization in our case were the high efficiency for both components of polarization in THz range and splitter handling simplicity. In order to simplify alignment of the interferometer the radiation incidence angle was chosen to be 45 degree. In Fig.2 the dependence of the beam splitter efficiency for both components of polarization on the radiation frequency is presented.

As can be seen from the figure in case when the silicon splitter thickness is several hundred micrometers, the beam splitter efficiency curve has many closely spaced cycles (as shown on Fig.2). What affects spectrum measurements and should be taken into account for high resolution spectroscopy. In other words the frequencies which have very low beam splitter efficiencies are excluded from interference and hence do not appears in the reconstructed spectrum. However, if the spectrometer resolution is less than the cycle's period, the only average beam splitter response will be observed. So the best

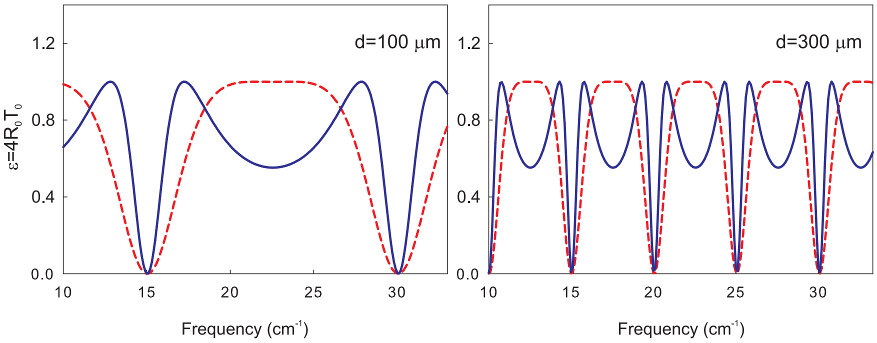

Figure 2: Variation in the efficiency of 100 μm and 300 μm silicon beam splitters as a function of wavenumber for s- and p-polarized radiation (solid and dashed curves, respectively).

way to measure broadband spectrum with high resolution is to have a set of splitters with different thickness.

In our experiment we have used commercially available 300 ± 10 μm thick, 150 ± 0.5 mm diameter n-type (Boron doped) Si plate, which has two polished surfaces. The chemical polishing technique provides the surface roughness much less than a radiation wavelength, what is far below tolerance requirements. The splitter smooth edges allows to decrease influence of the diffraction effect onto measured autocorrelation dependence.

2.2. Motion system

Motion system directly affects spectral measurements quality. It should have sufficient mechanical resolution, stability, repeatability and compatibility with modern hardware and software controllers. Moreover it should be calibrated and its linearity should be checked with high precision.

To estimate mechanical resolution and travel range of the motion system, required to measure a certain frequency spectrum with a MI, one should consider target spectral resolution and radiation spectral bandwidth. To be able to determine radiation spectrum in a range of $0.1 - 4$ THz with 10 GHz resolution one need to consider a motion system with 19.2 μm resolution and 15 mm minimal travel range

The ultra-high precision Kohzu YA16A-R1 stepping motor-powered, 0.1 μm resolution linear stage based on cross-roller guide with ground-screw lead mechanism [35] was chosen to design a movable arm of the interferometer. The stage was equipped with a non-contact incremental optical linear encoder (Renishaw RGH24 [36]) with 50 nm resolution. Such high resolution has enabled us to control the mirror M2 position even when we perform alignment of the interferometer with the 632 nm wavelength laser.

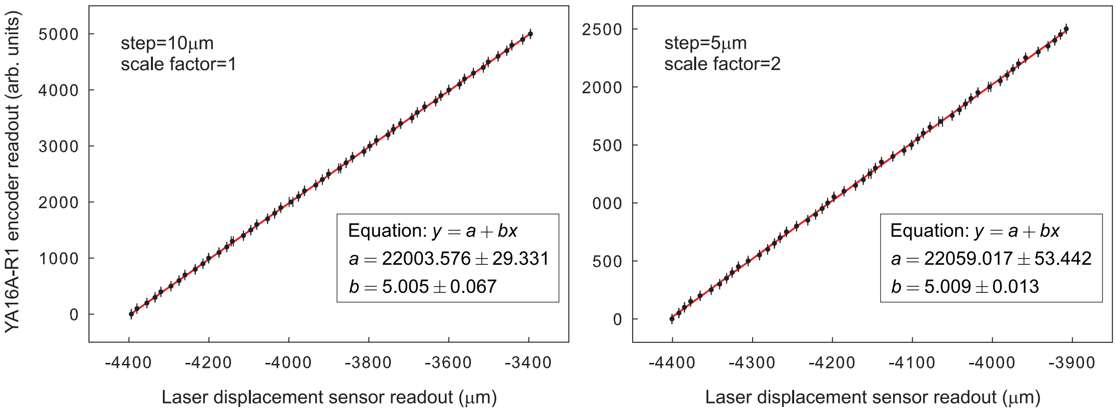

Figure 3: Typical calibration curves of motorized stage for different steps and scale factors.

The motor was controlled by an industrial-grade Oriental Motor CRK-series controller [37] in the open-loop mode (i.e. with no feedback). It has a simple programmable interface via RS-485 communication protocol and allows daisy-chain of up to 32 motion controllers, what makes it unifying solution for the LUCX THz program where many other motion mechanisms are foreseen. The controller supports micro-step motor operation mode so it is possible to change the real motor step angle by changing number of micro-steps per step. In this case the motor's base step angle should be divided by a corresponding scale factor. If the base step angle of the motor is 0.72 degree/step the value of the scale factor could be changed from 1 to 250 that corresponds to 0.72 degree/step and 0.00288 degree/step respectively. In this case the actual resolution of the motion system is determined by a combination of mechanical resolution of the linear stage, stepping motor quality/grade and electrical noise in the motion controller/driver. In order to verify resultant resolution, stability and backlash the constructed motion system was cross-calibrated against Keyence LK-G30 [38] high-accuracy CCD-laser displacement sensor, which has 0.01 μm absolute resolution and $\pm$0.05 % linearity. The results of the high precision motorized stage calibration for different scale factors are presented in Fig.3.

As expected, the linearity of the calibration curves does not change for different scale factors. The 0.2 μm resolution in micro-step mode was observed when the scale factor was equal to 20. The backlash value was measured to be less than 0.5 μm.

2.3. Alignment system

The microwave interferometers are rather sensitive for alignment, especially when they are operated in THz frequency range. In this case the alignment accuracy scales with the radiation wavelength and the intricacy level of alignment is increased. Inaccurate adjustment of any element could cause to variation of the light path. It implies the quality degradation of the recorded autocorrelation. There are two effects that tend to degrade the modulation intensity: mirror misalignment and non-parallel incoming radiation beam, i.e. when two beam splitting take place at different positions on the BS causing degradation of the phase map of the wavefront and, as a result, the measured autocorrelation. The combined effect also leads to interferogram asymmetry as well as to a degradation of modulation intensity [39].

There are two common alignment techniques which are widely used for opto-mechanical systems alignment and can be directly applied for THz interferometer: geometrical referencing and "cold-test" alignment. First one includes just geometrical alignment of the optical elements (or its holders) with respect to known mechanical references with the help of a standard alignment tools like levels, scales, measures, etc. The "cold-test" is in fact more accurate technique which requires to substitute an actual radiation beam with the test source beam to perform alignment or even calibration of the system. Unfortunately THz test sources are quite expensive and require additional care significantly increasing overall system complexity. Also it is always preferable to have compact and build-in alignment system for a quick and high quality system justification.

We decided to use helium-neon laser (NEC GLG 5240) as a primary alignment tool. A special interferometer splitter base magnetic mounting pairs were ordered to be able to replace Si splitter with an optical splitter (Sigmakoki CSMH 40-550) without disturbing its angular alignment with respect to interferometer axes. The additional periscope and a defocusing system for alignment laser were also introduced. The unpolished side of the optical splitter (OS) was used as a screen for visual control of the interferometer alignment.

The goal of the high precision alignment was to observe the interference fringe pattern produced by the He-Ne laser light on the unpolished side of the

OS. Similar to the description in the beginning of the section, alignment laser beam was splitted in two path and the splitted beams were directed towards the screen, interfered and produced a fringe pattern [40]. This pattern was used for precise interferometer axis and mirrors angular misalignment checks, Fig.4.

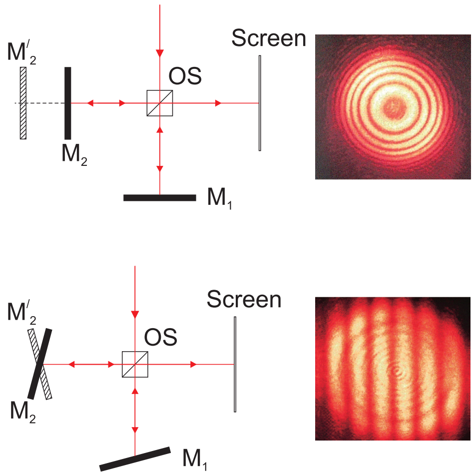

Figure 4: Formation scheme of fringes in MI (left) and the obtained fringe pattern photograph (right).

A half of the initial alignment laser beam returns back from the interferometer and travels through the THz transport line and vacuum window of the LUCX electron beam line. Thus the alignment scheme also allows to verify that main interferometer optical axis is parallel to the emission axis of the THz radiation generated by the electron beam.

After that OS with half of the magnetic mount was replaced with Si splitter on another half of the magnetic mount and reflection path was re-checked.

2.4. Schottky-barrier diode detectors

To detect the far-infrared coherent radiation, two different ultra-fast highly sensitive room-temperature detectors were used. The first was a Schottky Barrier Diode (SBD) detector with the rated frequency response range of $60 - 90$ GHz [41]. The second was a Quasi-Optical Broadband Detector (QOD) based on Schottky Diode with folded dipole antenna with the frequency response range of $100 - 1000$ GHz [42]. The basic parameters of these detectors are listed in Table 1.

The Schottky diode detectors have a long history in electromagnetic radiation detection in the range from millimetre to THz waves. These are the rectifier-type detection devices, which normally consist of metallic contact layer deposited on a lightly doped semiconductor material grown on a heavily doped conducting substrate [43]. At incoming EM wave the electrons of the epitaxial layer can cross the depletion barrier firmed in the vicinity of the metal, causing current to flow in the device by two processes: thermal activation over the barrier or quantum-mechanical tunneling through the barrier. For Schottky-barrier diode detectors operated at room temperature, thermionic effects are dominant [44]. By its nature, such a devices have very short response time because it uses majority-carrier current flow and the recovery time associated with minority-carrier injection is absent [45, 46]. Detectors have rather flat frequency response, as their sensitivity shows minor variation over the entire wave band. As already mentioned, a detector operation at ambient temperature and an extremely fast response time make Schottky-barrier diode detectors more attractive in comparison with other room temperature detectors, such as Golay cells or pyroelectric detectors[47, 48, 49].

Detector	Parameter	Value
Schottky Barrier Diode detector	Frequency Range	$60 - 90\,\mathrm{GHz}$
	Wavelength range	$3.33 - 5\,\mathrm{mm}$
	Response Time	$\sim 250\,\mathrm{ps}$
	Antenna Gain	$24\,\mathrm{dB}$
	Input Aperture	$30 \times 23\,\mathrm{mm}$
	Video Sensitivity	$20\,\mathrm{mV/mW}$
Schottky Diode Quasi-Optical detector	Frequency Range	$0.1 - 1\,\mathrm{THz}$
	Wavelength Range	$0.3 - 3\,\mathrm{mm}$
	Response Time	Sub-ns
	Antenna directivity	$25 - 35\,\mathrm{dB}$
	Video Sensitivity	$500\,\mathrm{V/W}$

Table 1: Parameters of Schottky Diode detectors.

The QOD is a relatively new product on the market. To our knowledge this is its first experimental performance verification for short-pulse coherent radiation detection. It is important to mention that the detector outer dimensions and apertures were different since SBD was used with 22×14

mm aperture gain horn antenna and QOD was, by default, equipped with a 10 mm diameter Si lens. Nevertheless custom detector holders were used in order to keep both of them at the same centreline while testing.

The SBD and QOD signals were acquired synchronously with Inductive Current Transformer signal by a 1 GHz bandwidth, 5 GS/s Tektronix 685C Oscilloscope.

3. Experimental setup

For initial MI trial a test setup at KEK LUCX facility was constructed. The interferometer was set to measure coherent transition radiation (CTR) spectrum generated from one of the standard LUCX screen monitor. When the electron beam with parameters summarized in Table 2 passes through the center of the 50 × 50 mm aluminium plate oriented at 45 degrees with respect to the beam line it generates backward CTR with broad spectrum [50, 51]. The radiation propagates through a 90 mm (clear aperture) z-cut crystalline quartz vacuum window and is transported by a pair of the off-axis parabolic mirrors to the MI as shown in Fig.1. The photograph of the experimental setup is shown in Fig.5.

Parameter	Value
Beam Energy	8 MeV
Intensity/bunch, typ.	1 nC
Bunch length, max	10 ps
Bunch length, min	50 fs
Repetition rate, max	12.5 train/sec
Normalized emittance, typ	$4.7 \times 6.5\,\pi$mm mrad

Table 2: LUCX, RF Gun section beam parameters.

For infrared applications quasi-optical lenses made of low-loss materials like polyethylene, polypropylene or Teflon are frequently used for the purpose of focusing nearly parallel beams or for parallelizing light from a point source. Parabolic mirrors have certain advantages over these diffractive elements that make them indispensable especially for the use with far-infrared radiation. Firstly, a very good reflectivity of polished metal surface prevents absorption losses that inevitably occur in any lens material. Secondly, chromatic aberration does not appear, so the focal point is the same for light of all wavelengths [17].

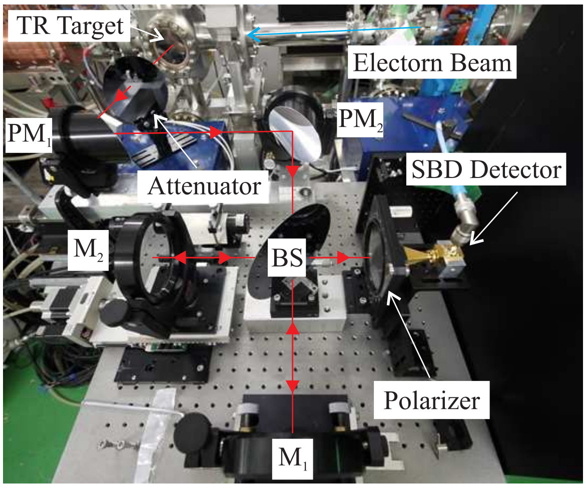

Figure 5: The photograph of the experimental arrangement.

In our case RTL consisted of a pair of 90 degrees off-axis parabolic mirrors. It was designed to form a parallel THz radiation beam without introducing any spectral distortions. The distance between parabolic mirrors defined by the divergence of the initial beam was simulated by Zemax software which allows to design, analyse and optimize different optical system for broad area of applications [52]. The commercially available 101.6×76.2 mm 90 degree off-axis alumina parabolic mirrors [53] with 152.4 mm effective focal length were used. The angle of transition radiation divergence is determined by the charged particle beam energy as γ^{-1}, where γ is the Lorentz-factor of the charge. The distance between radiation source and the first parabolic mirror could not be shorter than 600 mm due to supporting equipment allocation near the test setup. Thus we optimized only the distance between the parabolic mirrors. The main simulation quality criteria were the dimension of the final beam spot and its divergence throughout the RTL. The best result was obtained when the distance between off-axis parabolic mirrors was equal to 360 mm (see Fig.1). Thereby the overall acceptance angle of the spectrometer system is determined by the position of the first parabolic mirror (PM1) against the radiation source which was about 0.1 rad for both, horizontal and vertical directions.

4. Experimental results

Experimental investigation was done using a step-by-step approach and pursues several goals: QOD signal check, QOD and SBD polarization sensitivity and linearity tests, narrowband and broadband spectrum measurements. SBD signal level, polarization sensitivity and linearity check were previously performed in the course of a different experiment [22, 54] and were repeated here for a reference.

The detector polarization sensitivity, linearity and the saturation threshold are important parameters to obtain reliable experimental data. To investigate these detector characteristics the wire grid polarizers are usually used, since they are simple and reliable components which responds to just one polarization and are limited to radiation frequency which depends on size of wires and grid period [55, 56]. To evaluate polarization sensitivity of these detectors, 60 μm wire spacing and 15 μm wire diameter polarizer [57] with a slight tilt with respect to the radiation propagation path was installed in front of the detector. Using the same experimental setup and electron beam condition the signal for both horizontal and vertical SBD detector orientations was observed. From the oscilloscope traces shown in Fig.6 it is clear that the SBD detector is polarization sensitive. As expected QOD does not show such strong polarization sensitivity since the folded dipole antenna is much less sensitive for EM radiation polarization than the waveguide taper transformer of the SBD [58].

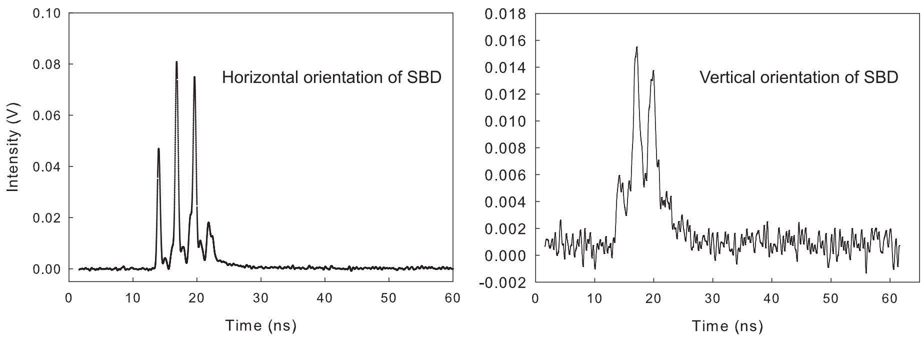

Figure 6: Observed signal for horizontal (right) and vertical (left) orientation of Schottky Barrier Diode Detector.

The QOD detector was equipped with an external RF circuit since it is susceptible to damaging electrostatic discharge (ESD) from the peripherals. However, the addition of an external protection device can slow the detector responsivity, leaving researchers with a need to balance the safety of the device and the measurement accuracy. To demonstrate the ESD protection circuit effect onto the QOD signal two sets of data with and without the ESD protection (see Fig.7) were taken for the same experimental conditions. The QOD signal measured without external ESD protection shows much faster response with almost the same signal intensity.

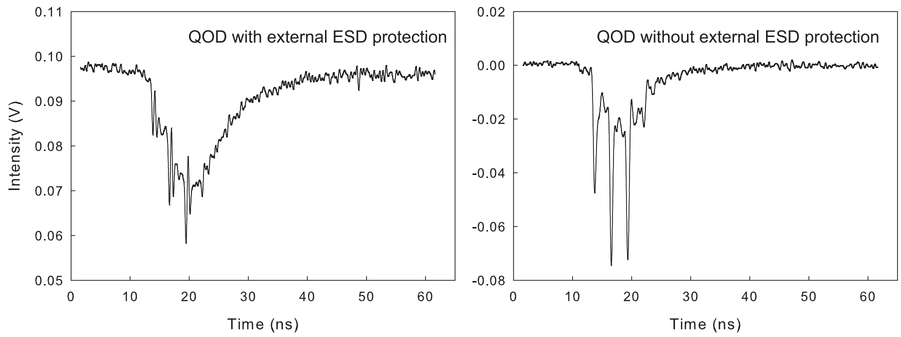

Figure 7: Observed signal of Quasi-Optical Broadband Detector with (right) and without (left) the ESD protection circuit.

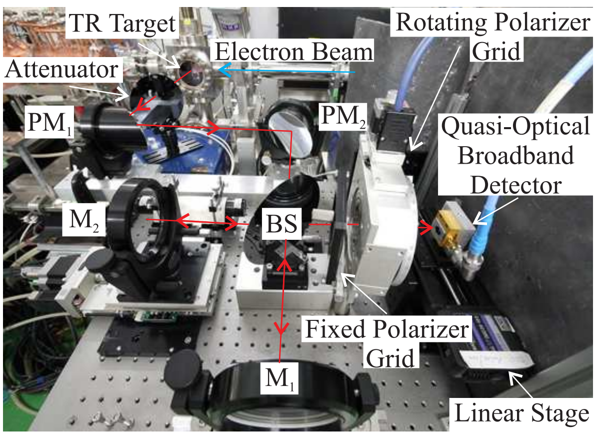

Figure 8: The photograph of the wire grid polarizers installation for linearity tests of SBD and QOD detectors.

The tests of the SBD and QOD detectors linearity were performed by placing two wire grid polarizers in front of the transition radiation source. The first polarizer was fixed and used to transmit one linear polarization at a time. The second polarizer was installed into remotely controlled motorized rotation stage (the arrangement of polarizers is illustrated in Fig.8). To check detectors linearity the dependence of horizontally polarized radiation intensity as a function of the motorized polarizer orientation angle θ was acquired. The measured correlation was approximated by the sine-like function. Figure 9 shows the linearity plot where the radiation intensity was presented versus the approximation sine function. The linear fits show a good linearity of both SBD and QOD detectors in the given response voltage range. Here, the upper limit of the linear response region is dictated by the detector saturation threshold. The lower limit of the linear response region corresponds to the minimum detectable signal level. As can be found from Fig.9 the SBD detector has a good linear response in the range from 0.02 V to 0.09 V, while QOD from 0.01 V to 0.045 V what corresponds to $0.1-4$ μW and $20-40$ μW input radiation power respectively. Thereby, the detectors provide an output voltage which is directly proportional to the power level of an RF signal without any external DC bias.

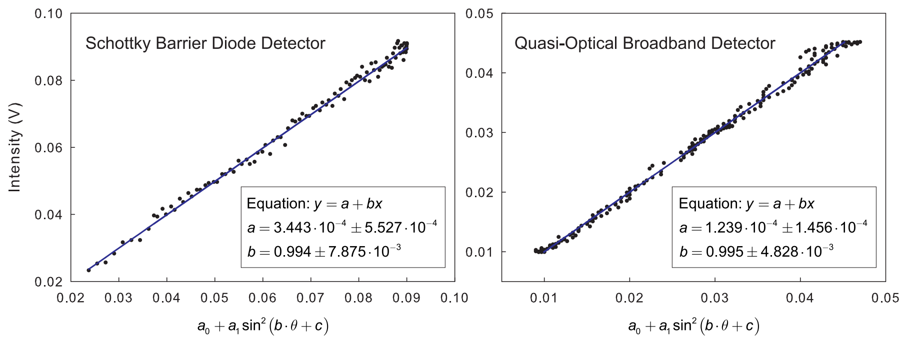

Figure 9: The measured linearity curves of the Schottky Barrier Diode detector (right) and Quasi-Optical Broadband detector (left).

After the input radiation power level was adjusted in order to avoid detectors saturation, autocorrelation dependencies were measured for both SBD and QOD detectors. To make interferograms from the raw oscilloscope traces the method based on analysis of the signal peak integrals that corresponded to an instantaneous transition radiation power of every electron bunch within the train was used. In this case the applied method permits measuring interferogram for any electron bunches in the train. To do so, the signal was averaged over twenty successive pulses of second bunch in the train for each M2 position set point. A typical SBD autocorrelation curve is presented in

Fig.10 (left). The M2 movable mirror translation step was 200μm. A symmetric form of the interferogram and a clear presence of several oscillation periods are a good evidence of a reasonable mirror alignment and motion stability.

To reconstruct the CTR spectrum from the measured autocorrelation data the method described in the reference [17] was used. As shown in Fig.10 (right), the restored spectrum is limited by the SBD spectral sensitivity range (see Table 1) and shows only beginning of the co-called "coherent threshold" around $70 - 100$GHz. Nevertheless obtained spectrum is consistent with our expectations about SBD spectral response and LUCX bunch length.

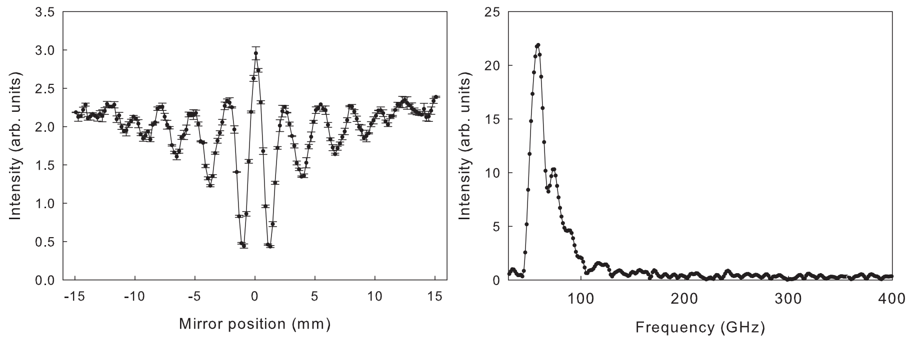

Figure 10: Schottky Barrier Diode detector intensity normalized by current as a function of the mirror position (left) and the restored spectrum (right).

To measure the broadband CTR spectrum, the SBD detector was replaced by the QOD. The M2 movable mirror translation step was changed to 50 μm. For each mirror position, the detector signals for twenty successive pulses were averaged again. Figure 11 shows an autocorrelation curve measured by the QOD detector and corresponding reconstructed spectrum. The autocorrelation curve has reasonable degree of symmetry with the slight increase of detected intensity at the right-hand side of the interferogram. This may come from the microwave reflections somewhere in the measurement system and will be investigated in later experiments. Again, measured spectrum shows only beginning of the CTR spectrum cut-off.

The reconstructed spectrum (Fig.11, left) shows agreement with the measurements performed with SBD detector as no high frequency spectral components were observed. That clearly means that the CTR spectrum threshold is located at the beginning of the frequency response range of the QOD detector. That gives a good chance to observe the full coherent radiation

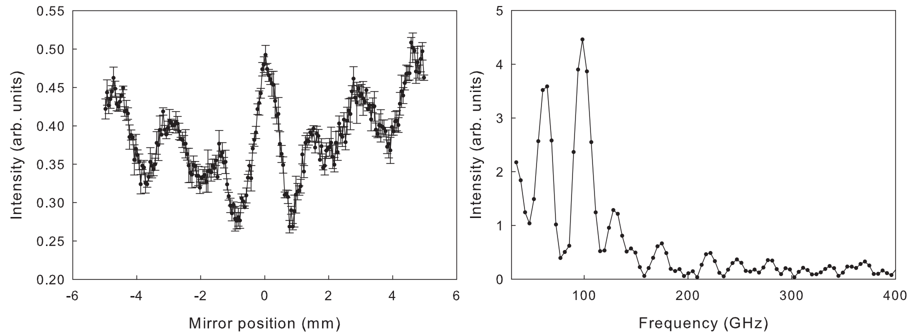

Figure 11: Quasi-Optical Broadband detector intensity normalized by current as a function of the mirror position (Right) and the restored spectrum (Left).

threshold for a much shorter electron bunches.

It is important to notice that both SBD and QOD detectors were used to determine CTR spectrum produced by each bunch of the 4-bunch 357MHz frequency train. This clearly shows that the constructed interferometer is capable to resolve busts of radiations separated minimum by $\sim$ 250ps (limited by detectors response), what can be used to determine bunch-by-bunch profiles of the multi-bunch train or characterize beam of the high repetition rate accelerators.

5. Conclusion and future plans

In this paper we present the initial Michelson Interferometer test and its performance investigation in THz frequency range. This apparatus has been constructed for intense THz radiation beams spectral measurements as a part of the larger program on THz sources development at KEK LUCX facility. The use of an ultra-fast highly sensitive Schottky Barrier Diode detector and a new Quasi-Optical Broadband Detector based on Schottky Diode with folded dipole antenna allowed for a detailed interferometer performance investigation. The QOD detector signal study shows that it has extremely fast response with relatively high sensitivity.

The major advantages of this instrument over existing THz spectrometers and commercial instruments is that it is capable to resolve busts of radiations separated minimum by $\sim$ 250ps (limited by detectors response), what can be used to determine bunch-by-bunch profiles of the multi-bunch train or characterize beam of the high repetition rate accelerators. Another advantage is simplicity, what potentially leads to high level of upgradeability without any special technical support and low price of the device. Also the large value of overall acceptance angle allows using interferometer for a numerous experimental investigations such as development of a wide angle THz sources and spectral-angular measurements.

For the first time the polarization response and linearity of the QOD in the pulsed mode was investigated. Also the simple and robust method to align Michelson Interferometer for THz spectral range using visual laser beam was implemented.

Our future plan is to produce a femtosecond micro-bunch train of electrons at KEK LUCX facility and use the MI as a main broadband spectra measurement tool for development of THz radiation source based on the different types of coherent radiation [21, 59]. At the same time the coherent spectrum information can be used for longitudinal beam size diagnostic and for the bunch shape reconstruction using Kramers-Kroning analysis [16, 17].

6. Acknowledgments

Authors would like to acknowledge assistance from ATF technical and scientific staff, and useful discussions with many of ATF-II collaborators. Also we would like to thank M. Tadano from Sigma-koki, M. Oke from Renishaw, H. Soga from Oriental Motors (Japan), F. Nagashima from AmTech, J. Hesler from Virginia Diodes and M. Ise from Edmund Optics (Japan) for their technical support of the project. Special thanks to Y. Honda for sharing his experience and for fruitful discussions. The work was supported by JSPS KAKENHI Grant number 23226020 and 24654076.

[1] S.W. Smye, J.M. Chamberlain, A.J. Fitzgerald and E. Berry, J. Phys. Med. Biol. 46 (2001) R101.

[2] P.H. Siegel, IEEE Trans. Microwave Theory Tech. 53 (2004) 2438.

[3] A.R. Orlando and G.P. Gallerano, J. Infr, Milli Terahz Wav. 30 (2009) 1380.

[4] T. Kampfrath, K. Tanaka and K.A. Nelson, Nature Photonics 7 (2013) 680.

[5] M.C. Hoffmann and J.A Fulop, J. Phys. D: Appl. Phys. 44 (2011) 083001.

[6] W.L. Chan, J. Deibel and D.M. Mittleman, Rep. Prog. Phys. 70 (2007) 1325.

[7] E. Mueller, Photonics Spectra 11 (2006).

[8] M. Gensch, Proc. FEL, New York, USA, 2013.

[9] K.W. DeLong, D.N. Fittinghoff and R. Trebino, IEEE J. Quantum Electron. 132 (1996) 1253.

[10] I. Amat-Roldan, I. Cormack and P. Loza-Alverf, Optic Express 12 (2004) 1169.

[11] www.hamamatsu.com

[12] S. Belomestnykh, I. Bazarov, V. Shemelin, J. Sikora, K. Smolenski and V. Vashcherevich, Nucl. Instr. Meth. Phys. Res. A 614 (2010) 179.

[13] www.radiabeam.com

[14] S. Matsuba, Y. Honda and T. Miyajima, Proc. IPAC, Kyoto, Japan, 2010, MOPE002.

[15] Bernd Richard Steffen, Diploma Thesis DESY 2007-020, DESY-THESIS 2007-020, 2007.

[16] A. Murokh, J.B. Rosenzweing, M. Hogan, H. Suk, G. Travish and U. Happek, Nucl. Instr. Meth. Phys. Res. A 410 (1998) 452.

[17] L. Frohlich, Diploma Thesis DESY 2005-011, FEL-THESIS 2005-02J, 2005.

[18] Y. Shibata, S. Hasebe, K. Ishi, T. Takahashi, T. Ohsaka, M. Ikezawa, T. Nakazato, M. Oyamada, S. Urasawa, T. Yamakawa and Y. Kondo, Phys. Rew. E 52 (1995) 6787.

[19] G. Geloni, E.L. Saldin, E.A. Schneidmiller and M.V. Yurkov, A method for Ultrashort Electron Pulse-Shape measurement Using Coherent Synchrotron Radiation, DESY, Hamburg, Germany, 2003.

[20] M. Catellano, V.A. Verzilov, L. Catani, A. Cianchi, G. Orlandi, and M. Geitz, Phys. Rev E 63 (2001) 056501.

[21] M. Fukuda, S. Araki, A. Deshpande, Y. Higashi, Y. Honda, K. Sakaue, N. Sasao, T. Taniguchi, N. Terunuma and J. Urakawa, Nucl. Instr. Meth. Phys. Res. A 637 (2011) S67.

[22] A. Aryshev, S. Araki, M. Fukuda, K. Lekomtsev, M. Shevelev, J. Urakawa, A. Potylitsyn and K. Sakaue, Proc. PASJ, Nagoya, Japan, 2013, SUP020.

[23] A. Aryshev, S. Araki, M. Fukuda, N. Terunuma, J. Urakawa, P. Karataev, G. Naumenko, A. Potylitsyn, L. Sukhikh, D. Verigin and K. Sakaue, 2013, arXiv:1310.7755.

[24] P.R. Griffiths and C. Homes, Handbook of Vibration Spectroscopy, John Wiley & Sons, Ltd, 2006.

[25] D.H. Martin and E. Puplett, Infrared Physics 10, (1969) 105.

[26] B. Reichborn-Kjennerud, Folloing the Polarization in a Martin-Puplet interferometer, Columbia University, 2004.

[27] G. Naumenko, A. Potylitsyn, G. Kube, O. Grimm, V. Cha and Yu. Popov, Nucl. Instr. Meth. Phys. Res. A 603 (2009) 35.

[28] E. Chiadroni, A. Bacci, M. Bellaveglia, P. Calvani, M. Castellano, A. Cianci, G.Di. Pirroi, M. Ferrario, G. Gatti, O. Limaj, S. Lupi, B. Marchetti, A. Mostacci, D. Nicoletti, A. Nucara, E. Pace, C. Ronsivalle, A.R. Rossi, C. Vaccarezza, Journal of Physics: Conference Series 357 (2012) 012034.

[29] www.sigma-koki.com

[30] D.A. Naylor, R.T. Boreiko and T.A. Clark, Appied Optics 17 (1978) 1055.

[31] C.C. Homes, G.L. Carr, R.P.S.M. Lobo, J.D. LaVeigne and D.B. Tanner, Appied. Optics 46 (2007) 7884.

[32] E.V. Loewenstein, D.R. Smith and R.L. Morgan, Applied Optics 12 (1973) 398.

[33] D.F. Edwards, Handbook of Optical Constants of Solids ed. E.D. Palik, Academic, 1985.

[34] R.J. Bell, Introductory Fourier transform Spectroscopy, Academic, 1972.

[35] www.kohzuprecision.com

[36] www.renishaw.com

[37] www.orientalmotor.com

[38] www.keyence.com

[39] L.W. Kunz and D. Goorvitch, Applied Optics 13 (1974) 1077.

[40] M. Born and E. Wolf, Principles of Optics 4^{th} ed. Pergamon Press, 1970.

[41] A. Aryshev, S. Araki, P. Karataev, T. Naito, N. Terunuma and J. Urakawa, Nucl. Instr. Meth. Phys. Res. A 580 (2007) 1544.

[42] www.vadiodes.com

[43] K.J. Button (Ed.), Infrared and Millimeter Waves, vol. 6, Academic Press, New York; Tokyo, 1982.

[44] H.C. Torrey, C.A. Whitmer, in: S.A. Goudsmit, et al. (Eds.), Cristal Rectifiers, Boston Technical Publ., Lexington, MA, 1964.

[45] H.A. Watson (ED.) Microwave Semiconductor Devices and their Circuit Applications, McGraw-Hill, New York, 1969.

[46] IEEE Transaction on Microwave Theory on Microwave Theory and Techniques, vol. MTT-14, No. 12, 1966.

[47] J.L. Hesler and T.W. Crowe, Proc. 18^{th} Intl. Symposium on Space Terahertz Technology, Pasadema, CA, 2007, 100.

[48] P.R. Griffiths and J.A. Haseth, Fourier transform infrared spectrometry, New York: Wiley interdcience, 209, 1986.

[49] P.R. Griffiths and C.C. Homes, Instrumentation for far-infrared spectroscopy, Handbook of Vibration Spectroscopy, Theory and Instrumentation vol. 1, New York: Wiley, 2001.

[50] V.L. Ginzburg and V.N. Tsytovich, Transition Radiation and Transition Scattering, Adam-Hilger, New York, 1990.

[51] A.P. Potylitsyn, M.I. Ryazanov, M.N. Strikhanov and A.A. Tishcenko, Diffraction Radiation from Relativistic Particles, Springer, Berlin, 2010.

[52] www.zemax.com

[53] www.edmundoptics.com

[54] A. Aryshev, D. Verigin, S. Araki, M. Fukuda, P. Karataev, G. Naumenko, A. Potylitsyn, S. Sakaue, L. Sukhikh, N. Terunuma and J. Urakawa, Proc. 7^{th} IFOST, Tomsk, Russia, 2012, 6357788.

[55] www.specac.com

[56] www.teraherz.co.uk

[57] www.amtechs.co.jp

[58] S. Silver, Microwave Antenna Theory and Design, New York: Dover, 1965.

[59] I. Konoplev, A. Aryshev, J. Urakawa, K. Lekomtsev, M. Shevelev and A. Seryi, Proc. 38^{th} Inter. Conf. IRMMW-THz, Mainz, Germany, 2013.